



**HAL**  
open science

# Depth profile analysis and high-resolution surface mapping of lithium isotopes in solids using laser-induced breakdown spectroscopy (LIBS)

Doriane Gallot-Duval, Céline Quere, Eric de Vito, Jean-Baptiste Sirven

## ► To cite this version:

Doriane Gallot-Duval, Céline Quere, Eric de Vito, Jean-Baptiste Sirven. Depth profile analysis and high-resolution surface mapping of lithium isotopes in solids using laser-induced breakdown spectroscopy (LIBS). *Spectrochimica Acta Part B: Atomic Spectroscopy*, 2024, 215, pp.106920. 10.1016/j.sab.2024.106920 . cea-04607774

**HAL Id: cea-04607774**

**<https://cea.hal.science/cea-04607774>**

Submitted on 11 Jun 2024

**HAL** is a multi-disciplinary open access archive for the deposit and dissemination of scientific research documents, whether they are published or not. The documents may come from teaching and research institutions in France or abroad, or from public or private research centers.

L'archive ouverte pluridisciplinaire **HAL**, est destinée au dépôt et à la diffusion de documents scientifiques de niveau recherche, publiés ou non, émanant des établissements d'enseignement et de recherche français ou étrangers, des laboratoires publics ou privés.

**Title:** Depth profile analysis and high-resolution surface mapping of lithium isotopes in solids using laser-induced breakdown spectroscopy (LIBS)

**Authors:** Doriane Gallot--Duval ([doriane.gallot-duval@cea.fr](mailto:doriane.gallot-duval@cea.fr))<sup>1</sup>, Céline Quéré<sup>1</sup>, Eric De Vito<sup>2</sup>, Jean-Baptiste Sirven<sup>1</sup>

<sup>1</sup>*Université Paris-Saclay, CEA, Service de Physico-Chimie, 91191 Gif-sur-Yvette, France*

<sup>2</sup>*Univ. Grenoble Alpes, CEA, Liten, 38000 Grenoble, France*

### **Abstract**

Lithium isotopic analysis is of interest in various fields from biology to energy. In addition to analytical methods commonly used for that purpose, a new complementary method for determining the spatial resolution of isotopic ratio in solid samples was previously developed: laser induced self-reversal isotopic spectrometry (LIBRIS), derived from laser-induced breakdown spectroscopy (LIBS). In this paper, we present a proof of concept of fast spatially-resolved quantitative isotopic analysis of lithium by LIBS both in depth (z resolution) and in configuration of high-resolution surface mapping (x and y resolution). First, a depth profile measurement where a 9% relative uncertainty on the <sup>6</sup>Li isotopic ratio and 0.74 μm depth resolution is obtained. Then, we introduce the first high-resolution lithium isotopic mapping obtained by LIBS with a 3.3 μm lateral resolution and a typical 40% relative uncertainty on the <sup>6</sup>Li isotopic ratio is obtained. Those results could be applied in the future to a large number of solid samples where fast information on the lithium isotopic distribution are needed, for instance in solid-state batteries development.

**Keywords:** lithium, isotopic analysis, LIBS, high-resolution mapping, depth profile measurements

## 1. Introduction

Isotopic analysis in solids is commonly performed after sampling, dissolution, chemical preparation, followed by mass spectrometry. This approach strongly limits the spatial resolution of the analysis at the sample scale. Yet, spatially-resolved isotopic measurements, i.e. depth profiles and/or surface mapping, can deliver crucial information when the sample is inhomogeneous or structured at the micrometric scale or even smaller. In the energy field, spatially-resolved isotopic measurements are used for instance to study Li-ion pathways in lithiated materials using isotopic labelling [1–3], and they are also of particular interest in organ and tissue bio-imaging and metabolic activities study [4,5]. Such measurements are powerful tools to investigate the geochemistry and geochronological dating of various materials [6–8]. One last example of the utilization of spatially-resolved analytical techniques is nuclear non-proliferation, e.g. to study the homogeneity of uranium containing samples to recover information on the production process [9].

To enable these analyses, various techniques can be used. A few examples are briefly reviewed in the case of lithium, a strategic element for energy storage applications. For depth profile measurements, Glow Discharge Mass Spectrometry (GD-MS) provides a depth resolution in the nanometer range – and a centimetric lateral resolution [3]. This technique has a ppb detection limit [10] and a 1% mass resolution for lithium was reached [11]. Some of the most precise techniques in the three dimensions are extreme ultraviolet laser ablation and ionization mass spectrometry (EUV MS) that reached nanoscale resolution [12,13] and atom probe tomography (APT) [14] with a resolution in the nanoscale range as well [15]. The highest precision on the isotopic ratio is reached by Nanoscale secondary ion mass spectrometry (NanoSIMS) and laser ablation coupled with an Inductively Coupled Plasma Mass Spectrometry (LA-ICP-MS) (possibly coupled with multi-collector detection [16]) with respectively a < 1‰ on the lithium isotopic ratio [17] and 2‰ uncertainty on the carbon isotopic ratio [18]. Those techniques reach a sub-ppb detection limit for NanoSIMS [19] and a sub-ppm limit for LA-ICP-MS [8]. Spatial resolution of NanoSIMS (10 nm to 10 μm [12,20,21]) is higher than LA-ICP-MS (surface and depth resolution in the micrometric range [12,20,22,23]). Time of Flight Secondary Ion Mass Spectrometry (ToF-SIMS) is also a powerful analytical technique as it allows to perform analysis with a 100 nm to 10 μm lateral resolution [19,20], a nanometric depth resolution [24] and a ppm to ppb detection limit [19,24–26] and reach uncertainties lower than 1% on the lithium isotopic ratio [1,17]. Other analytical techniques based on laser ablation were used, such as laser ablation coupled to laser-induced fluorescence [27], which achieves an uncertainty of 4% on the lithium isotopic ratio, pseudocontinuum source atomic absorption spectroscopy (psCS-AAS) [28], Tunable Diode Laser Absorption Spectroscopy (TDLAS) [29] or laser-induced breakdown spectroscopy (LIBS) [30–32]. All these techniques were implemented at low or very low pressure, in order to limit the effects of spectral broadening [33]. For further information on optical systems for standoff isotopic analysis the review of Harilal et al. (2018) [33] is very complete.

As a complement to those analytical methods, a new technique called laser-induced breakdown self-reversal isotopic spectrometry (LIBRIS) was developed by Touchet et al. [34,35] to perform lithium isotopic analysis on solid samples without sample preparation. This technique uses either the wavelength of the self-absorption dip [34] or the wavelength of the emission line of the 670.8 nm lithium emission line. The wavelength of this line is indeed directly correlated to the lithium isotopic ratio. Touchet et al. [34,35] used a 50 μm laser spot on lithium carbonate ( $\text{Li}_2\text{CO}_3$ ) and reached a 6% relative uncertainty on the  ${}^6\text{Li}$  isotopic abundance. LIBRIS was then developed for the analysis of a solid polymer electrolyte part of solid-state batteries, with a crater diameter of 7 μm [36]. However, quantitation of the  ${}^6\text{Li}$  isotopic abundance required to accumulate 20 laser shots, therefore limiting high-resolution analysis to one-dimensional systems. In order to truly analyze 2D solid-state batteries

systems, in this paper we develop the LIBRIS technique in single-shot mode and with twice lateral resolution.

This paper presents the first development of the technique to perform fast spatially-resolved quantitative lithium isotopic analysis of solids, both in depth (z resolution) and in configuration of high resolution surface mapping (x and y resolution). Note that in the following sections of this article, we will simply refer to this technique as laser-induced breakdown spectroscopy (LIBS), as the acronym LIBRIS, originally created for the analysis of self-absorbed lines, is no longer relevant since the technique was shown to be applicable to emission lines [36].

## 2. Materials and methods

### 2.1. Experimental setup and measurement parameters

Two different LIBS systems operating with a 266 nm frequency-quadrupled Nd-YAG laser and a 1-m focal length Czerny-Turner spectrometer (Jobin-Yvon THR1000) equipped with an intensified charge coupled device (iCCD) camera (Andor iStar) were used. Both systems were presented in our previous work [36]. The focusing lens is a 200mm plano-convex lens for the low-resolution system and a x15 microscope lens (LMU-15X-266, OFR) for the high resolution system. The energy of the laser used for high lateral resolution analysis was reduced by the use of a laser beam attenuator and a diaphragm. The dimensions of ablation craters obtained on the samples were characterized using a white light optical profilometer (Bruker ContourGT). The acquisition parameters are summarized in Table 1 for both analyzes. Note that it was chosen to integrate temporally the plasma emission to collect more light, hence to have a better signal-to-noise ratio, than when using a time-resolved detection of the plasma. Also, the slit was strongly broadened for high resolution measurements, up to 540  $\mu\text{m}$ , in order to increase the plasma light collection efficiency. That was necessary since micro-ablation produced a very small and transient plasma.

*Table 1: measurement parameters for depth profile measurement and surface mapping*

	Depth profile measurement	Surface mapping
<b>Gate delay</b>	0 $\mu\text{s}$	0 $\mu\text{s}$
<b>Gate width</b>	100 $\mu\text{s}$	100 $\mu\text{s}$
<b>CCD exposure</b>	0.05 s	0.05 s
<b>Intensifier gain</b>	3000	3000
<b>Laser spot size</b>	50 $\mu\text{m}$	$\approx 1 \mu\text{m}$
<b>Number of laser shots per crater</b>	500	1
<b>Step between craters</b>	n.a.	7 $\mu\text{m}$
<b>Spectrometer slit width</b>	43 $\mu\text{m}$	540 $\mu\text{m}$
<b>Laser pulse energy</b>	5.3 $\pm$ 0.3 mJ	10 $\pm$ 0.5 $\mu\text{J}$
<b>Background gas atmosphere</b>	ambient air	argon

## 2.2. Samples

Epoxy containing lithium carbonate ( $\text{Li}_2\text{CO}_3$ ) samples were prepared by mixing two lithium carbonate powders, one with a natural isotopic abundance of lithium ( $7.5 \pm 0.1$  at. % of  $^6\text{Li}$ ) (Sigma Aldrich, purity > 99%), and one enriched in  $^6\text{Li}$  ( $95.5 \pm 0.1$  at. % of  $^6\text{Li}$ ) (Sigma Aldrich, purity > 99%). The powders were milled 15 min at a frequency of 30 Hz using a ball miller (Retsch, MM400). The resulting powder was then added to 1 mL of epoxy resin (Struers, ExpoFix) and stirred during 30 minutes using a magnetic stirrer. Then 0.130 mL of the hardening agent (Struers, ExpoFix) was added to the mixture and poured inside a 25 mm diameter mold. It was placed under vacuum atmosphere to remove bubbles and then left drying at atmospheric pressure and room temperature. Samples with variable  $^6\text{Li}$  isotopic abundance were prepared for calibration.

In order to demonstrate the ability to perform spatially-resolved isotopic measurements, both in depth and over the surface, two samples were assembled as presented on Figure 1, using the two commercial powders. The first sample was designed to allow performing z-axis analysis with a first layer smaller than the laser depth of field around the focal plane. The second sample was designed to present several interfaces between the different isotopic parts on a small surface. Then both samples were manually polished on abrasive paper and the last polishing was realized using a suspension of pyrogenic silica with  $0.25 \mu\text{m}$  diameter (Struers, OP-S NonDry) on a vibratory polisher (Buehler, VibroMet 2). The resulting samples are schematically represented on Figure 1.

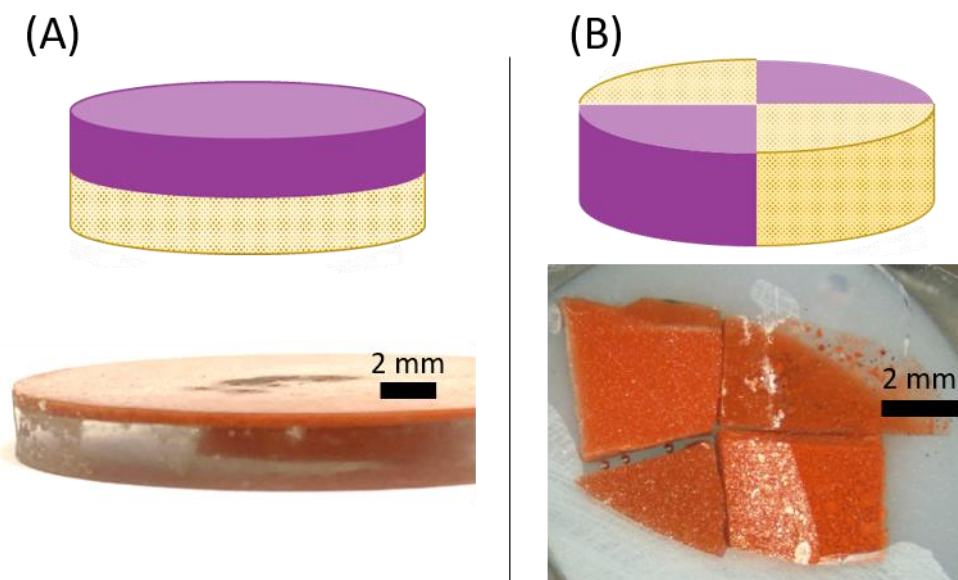


Figure 1: diagram and pictures of the prepared samples, 7.5%  $^6\text{Li}$  in purple, 95.5%  $^6\text{Li}$  in dotted yellow, (A) for depth profile measurement, (B) for surface mapping. The transparent part on each sample corresponds to epoxy resin containing no lithium carbonate.

The typical absolute uncertainty on the lithium isotopic abundance in prepared samples is less than 0.1%, it is mostly due to the uncertainty on the isotopic abundance of commercial powders.

### 2.3. Spectra treatment

The lithium transition line considered is the Li I  $2s^2-2p^2$  resonance line, since this line presents the largest isotopic shift of  $15.8 \pm 0.3$  pm [37,38] between the resonant doublets at 670.7760/670.7911 nm and 670.7918/670.8068 nm, respectively for  $^7\text{Li}$  and  $^6\text{Li}$  [39].

The isotopic measurement is based on the determination of the central wavelength of the doublet by spectral fitting. As it is well known in the LIBS literature, the line profile is a convolution between instrumental broadening (usually Gaussian), Stark broadening (Lorentzian) and Doppler broadening (Gaussian). In our case, since measurements were time-integrated, the contribution of Stark and Doppler broadening varied during the measurement and the resulting line profile was a complex convolution of those different contributions.

For depth profile measurements under ambient air, self-reversal was observed. As shown on Figure 2, in this case the line profile had a typical width of 500 pm. The instrumental Gaussian broadening was 12.5 pm, and the Doppler width was estimated to 20 to 30 pm for a plasma temperature of 5000 to 10000 K [40]. Therefore, the Lorentzian Stark broadening was clearly predominant and the line profile was fitted by two Lorentzian curves, one for the emission line and one for the absorption dip. The resulting fit was found satisfactory as illustrated on Figure 2B.

For high-resolution measurements under argon, the line was not self-reversed and had a typical width of 200 pm. In this case, the instrumental broadening was 150 pm due to the large slit width, and the instrumental profile was no longer Gaussian: it was a gate function. Consequently, neglecting the Doppler broadening like in the previous case, the resulting line profile was a convolution between the instrumental gate function and the Lorentzian Stark broadening. As shown on Figure 2C, we found that a single Lorentzian curve enabled to satisfactorily fit the spectrum.

Examples of fitted single-shot spectra for each lateral resolution are shown on Figure 2 (B) and (C).

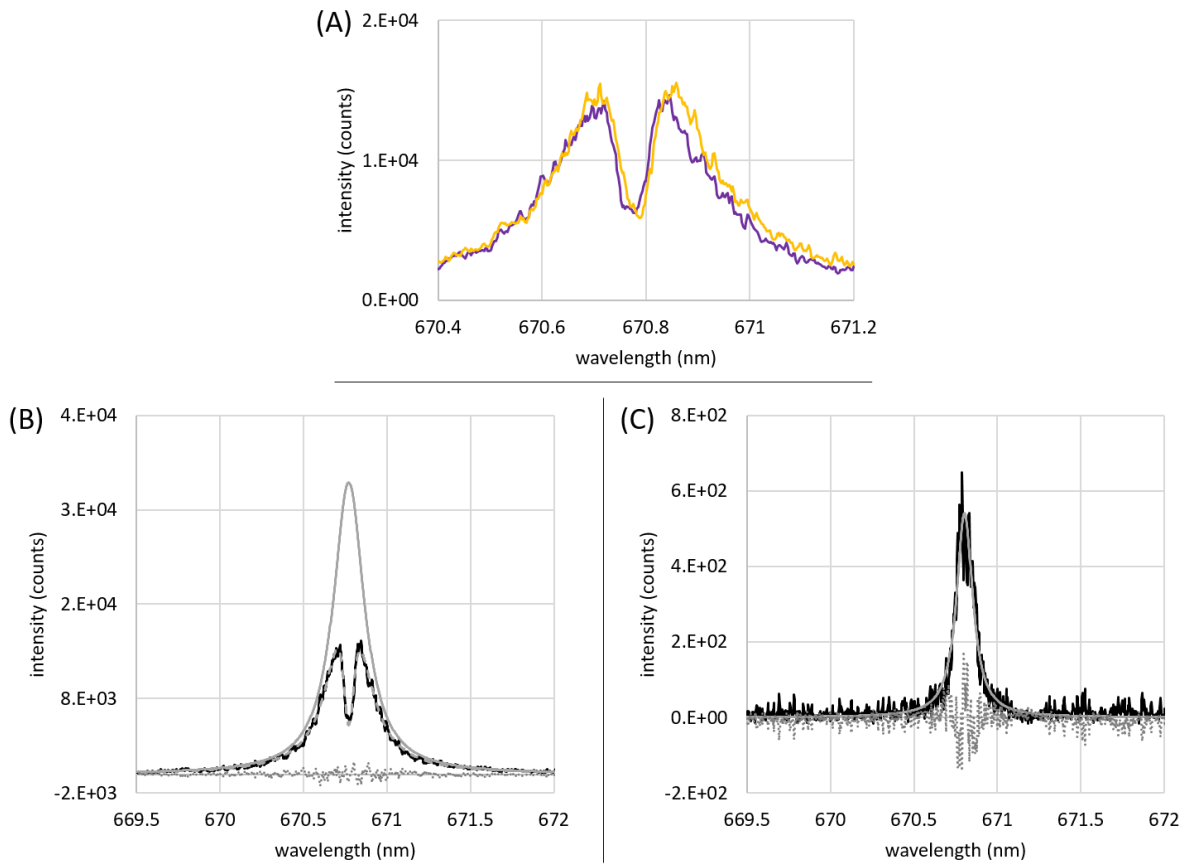


Figure 2: (A) single shot spectra of the Li I 670.8 nm line of epoxy containing  $\text{Li}_2\text{CO}_3$  with a 250  $\mu\text{m}$  lateral resolution at 7.5%  $^6\text{Li}$  in yellow and 95.5%  $^6\text{Li}$  in purple. (A,B) single shot spectra of the fitted single-shot spectra of the Li I 670.8 nm line of epoxy containing  $\text{Li}_2\text{CO}_3$  at natural abundance (7.5%  $^6\text{Li}$ ) with 250  $\mu\text{m}$  resolution (B) and 7  $\mu\text{m}$  resolution (C). Black continuous line: raw data, light grey continuous line: fitted Lorentz profile modelling the emission line, light grey dashed line: fitted reversed line combining the emission line and the absorption dip, grey dotted line: residuals.

The wavelength of the absorption dip or of the emission line is then used to determine the  $^6\text{Li}$  isotopic abundance. Figure 2 (A) presents spectra of 7.5% and 95.5%  $^6\text{Li}$ , the wavelength shift is clearly visible.

### 3. Results and discussion

#### 3.1. Depth-resolved lithium isotopic analysis

Our first objective is to demonstrate the feasibility of the depth-resolved isotopic analysis of lithium by LIBS on epoxy samples. Such an analysis would be useful with multi-layers containing different  $^6\text{Li}$  isotopic abundance samples. In order to estimate the ablation efficiency, Figure 3 presents the evolution of the crater dimension as a function of the laser shot number. The ablated depth decreases with the number of accumulated laser shots, on average it is about 0.74  $\mu\text{m}$  per laser shot for a 500-shot crater.

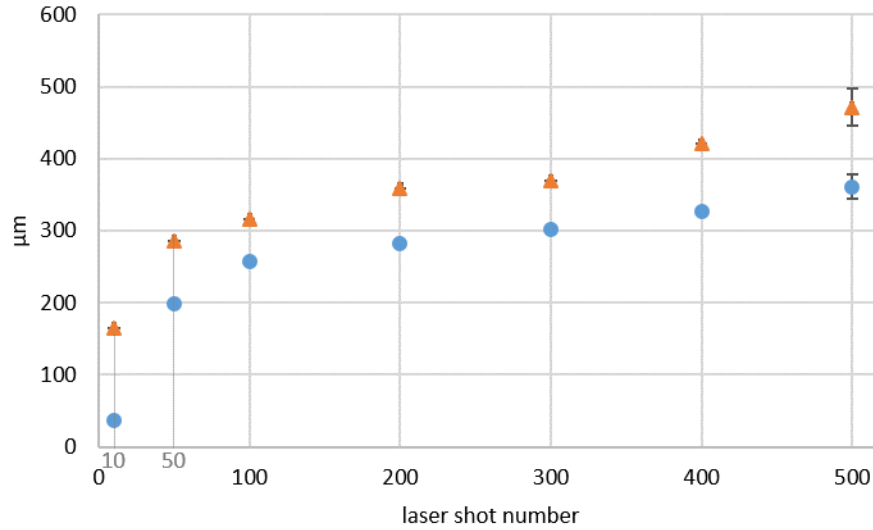


Figure 3: evolution of the crater depth (blue dots) and diameter (orange triangle) as a function of the laser shot number

To be able to quantitatively analyze the  ${}^6\text{Li}$  isotopic abundance in both layers of the epoxy sample A, a calibration curve on similar epoxy samples with variable lithium isotopic ratio was performed. In order to have the highest resolution in the z-axis, each measurement resulted from a single laser shot. The calibration results are presented in Table 2 and Figure 4.

Table 2: analytical performances of LIBS analysis of  ${}^6\text{Li}$  isotopic abundance in epoxy samples containing lithium carbonate with 500  $\mu\text{m}$  lateral resolution. a: slope of the calibration line, b: intercept,  $R^2$ : correlation coefficient,  $\Delta{}^6\text{Li}/{}^6\text{Li}$  (50%): relative uncertainty with 95% of confidence at 50% of  ${}^6\text{Li}$ .

	Theoretical values	Epoxy sample
<b>a (pm)</b>	$15.8 \pm 0.3$ [38]	$13.2 \pm 0.8$
<b>b (nm)</b>	670.7810	$670.782 \pm 0.001$
<b><math>R^2</math></b>	/	0.9904
<b><math>\Delta{}^6\text{Li}/{}^6\text{Li}</math> (50%) - single laser shot</b>	/	9%

The obtained calibration is consistent with the theoretical values and has a good correlation coefficient. Single-shot analysis leads to a relative uncertainty at 50% of  ${}^6\text{Li}$  of 9%, a satisfactory performance compared to our previous work on pure lithium carbonate samples, where an uncertainty of 6.0% was obtained for 20 accumulated laser shots [36]. As for the calibration line slope and intercept, in the absence of Stark and Doppler effects in the plasma, they are equal respectively to the isotopic shift between  ${}^7\text{Li}$  and  ${}^6\text{Li}$ , and to the wavelength of the  ${}^7\text{Li}$  line [34]. Those values are referred to as “theoretical values” in Table 2. Experimentally, for an unknown reason we obtain a calibration slope significantly lower than the theoretical one. In contrast, the experimental intercept is fully consistent with the theoretical one.

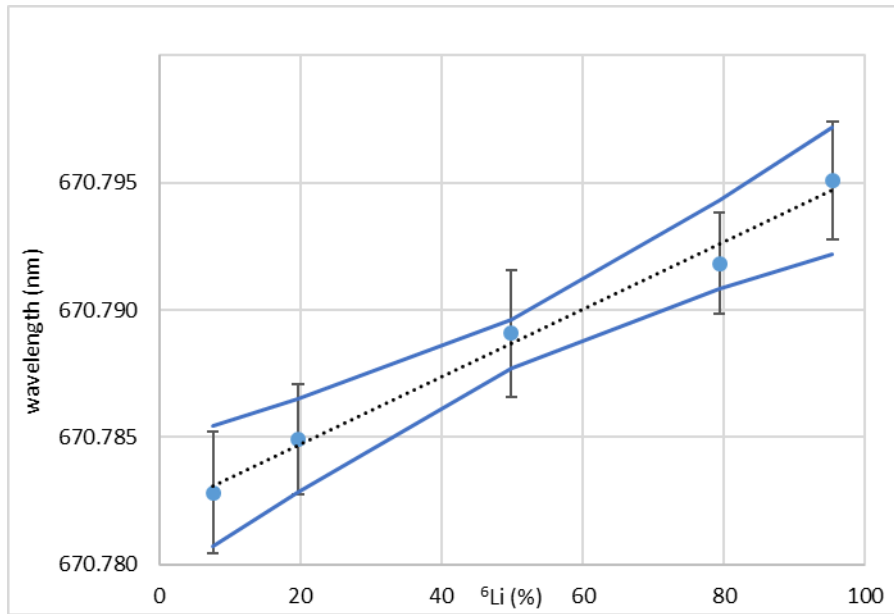


Figure 4: calibration curve of the  ${}^6\text{Li}$  isotopic abundance with 95% prediction bands, 500  $\mu\text{m}$  lateral resolution, single-shot measurements on epoxy samples containing  $\text{Li}_2\text{CO}_3$ . The wavelength of the absorption dip is plotted as a function of the isotopic abundance in  ${}^6\text{Li}$ . Error bars are equal to 2 standard deviations over the number of replicas. Absolute uncertainties on the lithium isotopic abundance in the samples are less than 0.1%

The next step was to perform a depth profile analysis of the two-layer epoxy sample presented in Figure 1 (A). 500 laser shots were achieved on each location, leading to craters of  $500 \pm 25 \mu\text{m}$  diameter and  $370 \pm 17 \mu\text{m}$  depth as shown on Figure 3. Then, single-shot spectra were analyzed separately. The  ${}^7\text{Li}$ -rich layer was on top of the  ${}^6\text{Li}$ -rich layer. Using a binocular magnifier, we measured the thickness of the  ${}^7\text{Li}$ -rich layer in the 4 cardinal points and found  $221 \pm 62 \mu\text{m}$ . So, according to Figure 3, we should reach this second layer after 50 to 200 laser shots.

Figure 5 shows the evolution of the wavelength of the absorption dip as a function of the laser shot number. Both layers are clearly visible between laser shots 0-180 and 320-500, with a transitional part in-between. From Figure 3, we note that 180 laser shots lead to an ablation depth of about 270  $\mu\text{m}$ , consistent with our visual estimation of the  ${}^7\text{Li}$ -rich layer depth. The obtained wavelength are coherent with the direction in which we have positioned the sample, with the low  ${}^6\text{Li}$  isotopic abundance on the top.

In the first layer, the mean wavelength corresponds to the measured wavelength of the calibration curve for natural lithium, i.e. with a 7.5%  ${}^6\text{Li}$  abundance. For the second layer, the wavelength is lower than the expected one observed for the 95.5%  ${}^6\text{Li}$  abundance on the calibration curve. This is explained by the Gaussian profile of the laser spot, leading to an ablation of the crater walls by the wings of the laser beam. This means that for each laser shot on the 95.5%  ${}^6\text{Li}$  layer we also ablate a part of the 7.5%  ${}^6\text{Li}$  layer, leading to an underestimation of the  ${}^6\text{Li}$  abundance. Another

phenomenon might induce a blue shift of the measured wavelength: a possible plasma confinement effect leading to a higher plasma density when the crater gets deeper, hence a stronger Stark effect. Yet, this might be limited considering the high diameter of the ablation crater compared to its depth.

The one sigma standard deviation on the three repetitions of the measurement is also increasing once we start shooting in the  ${}^6\text{Li}$ -rich layer. This is attributed to the increasing photon noise as the signal is lowering with the laser shot number.

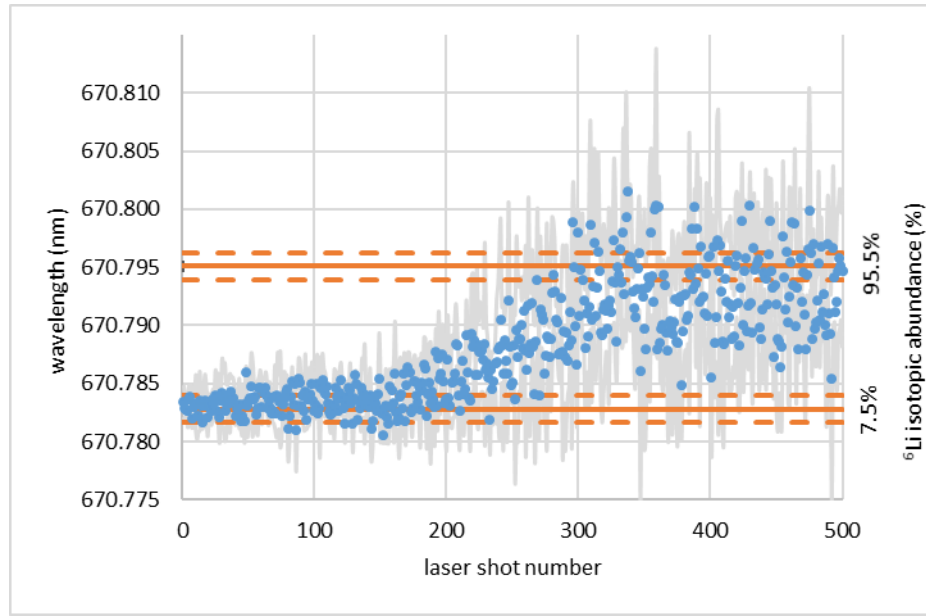


Figure 5: evolution of the wavelength of the absorption dip as a function of the laser shot number, blue dots: mean value of three repetitions, grey line: 1 sigma standard deviation of the three repetitions, orange line: 7.5% and 95.5% measured wavelength from the calibration curve, orange dashed line: uncertainty on the 7.5% and 95.5% measured wavelength from the calibration curve

Those results show that a depth-resolved isotopic measurement of lithium by LIBS is feasible, with a depth resolution lower than  $1\ \mu\text{m}$ , though with relatively large uncertainties. Such an analysis could be used to study large lithium isotopic variations in layered materials. To be able to measure steeper transitions and to avoid the underestimation of the deeper layer  ${}^6\text{Li}$  abundance, modifications could be made to the experimental setup in order to have a top-hat laser beam profile. Other methods exist for processing in-depth analysis results to determine phase transitions, such as Pearson 2D correlation plots [41,42]. In our case, however, this technique was not conclusive, as the shape of the spectra varies very little with isotopy.

To conclude, the resolution is far from the nanometer depth resolution from GD-MS [3] and 1% mass resolution from GD-MS [3,11], though the main advantage of LIBS for lithium isotopic analysis is that the sample does not need to be a good conductor, the lateral resolution is twice better than for GD-MS and the analysis is quite quick and easy to perform.

### 3.2. Lithium high-resolution surface isotopic mapping

The objective of this second part is to demonstrate the feasibility of a LIBS high-resolution surface mapping of the lithium isotopic abundance in an epoxy sample containing lithium carbonate. As we demonstrated in a previous work [36], the sample surface roughness is an important cause of measurement uncertainty when using a micro-ablation system. Therefore, the first step was to check that the polishing step was good enough to minimize surface irregularities (to be less than 10  $\mu\text{m}$  peak-to-peak). As presented on Figure 6 (A), we obtained a surface roughness of around 0.5  $\mu\text{m}$ . We also observed holes over the surface with a  $8 \pm 2 \mu\text{m}$  depth and a  $13 \pm 4 \mu\text{m}$  diameter. They were mostly due to trapped air bubbles in the resin. Single-shot laser ablation craters were analyzed to characterize the analysis spatial resolution and  $3.3 \pm 0.7 \mu\text{m}$  diameter and  $7.2 \pm 2.5 \mu\text{m}$  depth craters were obtained. They are presented on Figure 6 (B).

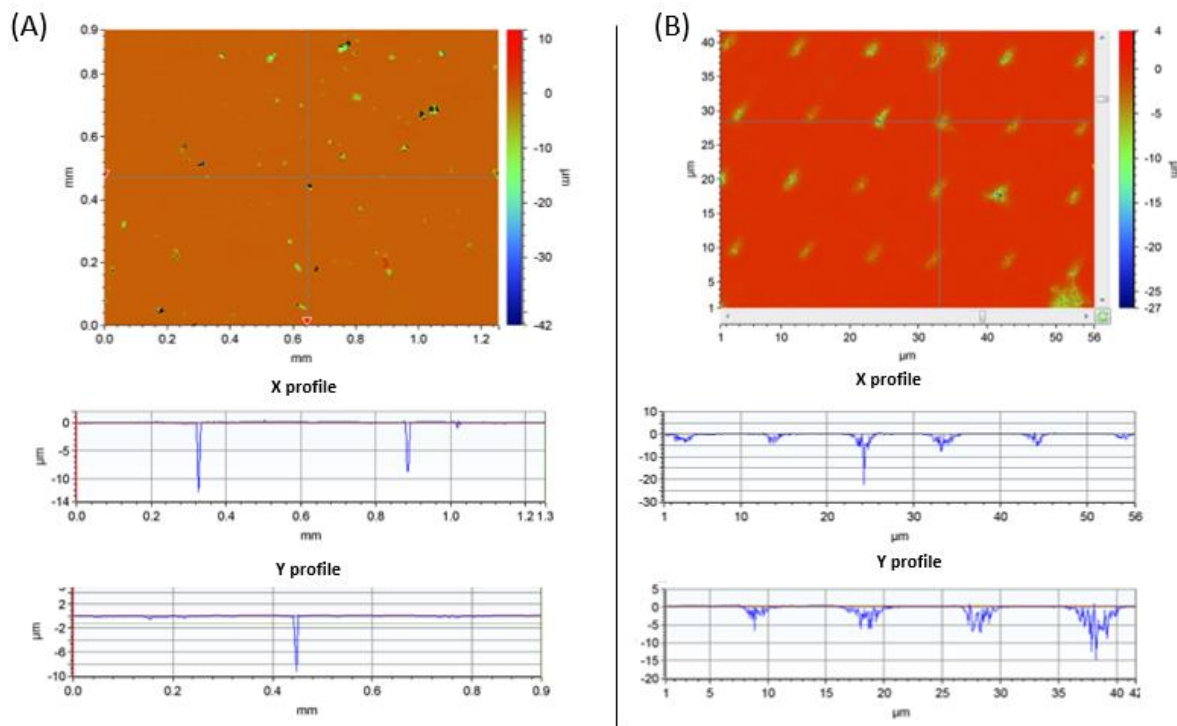


Figure 6: (A) profilometer analysis of an epoxy sample surface before ablation, (B) profilometer analysis of single-shot craters on epoxy samples using the high spatial resolution instrumentation. The apparent increasing depth of the Y profile is because craters are not perfectly aligned along the vertical direction.

Single-shot calibration curve results for epoxy samples with different lithium isotopic abundances are presented in Table 3 and Figure 7.

Table 3: analytical performances of LIBS analysis of  ${}^6\text{Li}$  isotopic abundance in epoxy samples containing lithium carbonate with  $3.3\mu\text{m}$  lateral resolution. a: slope of the calibration line, b: intercept,  $R^2$ : correlation coefficient,  $\Delta{}^6\text{Li}/{}^6\text{Li}$  (50%): relative uncertainty with 95% of confidence at 50%  ${}^6\text{Li}$ , FWHM: full width at half-maximum of the emission line.

	Theoretical values	Epoxy sample
<b>a (pm)</b>	$15.8 \pm 0.3$ [38]	$15.2 \pm 1.3$
<b>b (nm)</b>	670.7810	$670.778 \pm 0.001$

$R^2$	/	0.9786
$\Delta^6\text{Li}/^6\text{Li}$ (50%) - 20 accumulated laser shots	/	20%
$\Delta^6\text{Li}/^6\text{Li}$ (50%) - laser single shot	/	40%

Looking in detail at the calibration parameters, we see that the slope is consistent with the theoretical value. The intercept is a little bit lower than the theoretical value; therefore, a small blue shift occurs. It can be attributed to a matrix effect when ablating the epoxy resin. The relative uncertainty on the  $^6\text{Li}$  isotopic abundance in the mid-range of the calibration is of 20% when we consider the average of 20 laser shots, and of 40% when we consider the single-shot values. In comparison with the results previously obtained [36] on lithium carbonate with 30% relative uncertainty with 20 accumulated laser shots, the uncertainty was improved despite a lithium concentration about 5 times lower (100 %wt. against 21 %wt. in epoxy samples). Furthermore, the crater size was reduced from 11  $\mu\text{m}$  diameter and 3.5  $\mu\text{m}$  depth to 3.3  $\mu\text{m}$  diameter and 5  $\mu\text{m}$  depth, which induces a crater volume twice as small. Therefore, although the lithium ablated mass in the plasma is 10 times lower than for the lithium carbonate samples, we get an improvement of the relative uncertainty on the measurement. This is due to the lower roughness of the surface inducing an easier and better positioning of the sample in the laser focal plane. It indeed reduced an important source of uncertainty which was previously determined [36].

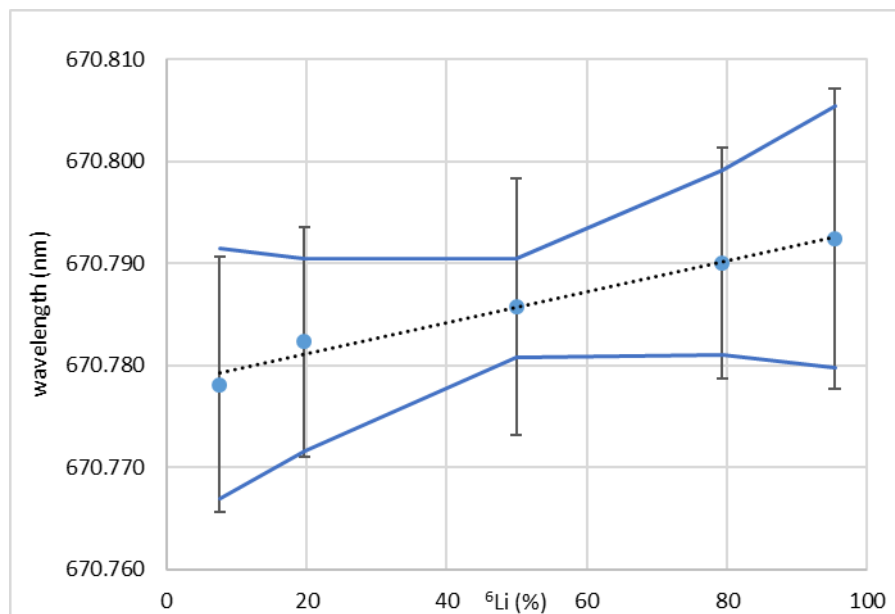


Figure 7: LIBS calibration curve of the  $^6\text{Li}$  isotopic abundance in epoxy containing  $\text{Li}_2\text{CO}_3$  with 95% prediction bands, 3.3  $\mu\text{m}$  lateral resolution, single-shot measurement. The emission line wavelength is plotted as a function of the isotopic abundance in  $^6\text{Li}$ . Error bars are equal to 2 standard deviations over the number of replicas. Absolute uncertainties on the lithium isotopic abundance in the samples are less than 0.1%.

Then, the sample presented in Figure 1 (B) was analyzed. A 350x350 single-shot mapping was realized, with a 7  $\mu\text{m}$  step, in the junction of the four sample parts, the analysis lasted  $\sim 3\text{h}30$ . An image of the analyzed area is shown on Figure 8 (A). The transparent parts are epoxy without lithium carbonate due to the difficulty to have a close contact between four solid sample parts.

Each single-shot spectrum was fitted using a simple Lorentz function and using the previously presented calibration curve, the isotopic abundance corresponding to the wavelength of the emission line was calculated. As no lithium was present on some parts of the mapping, a 575 counts background threshold was introduced to keep the spectra only where a significant lithium signal appeared, the background mean value being 540 counts. The resulting mapping is presented in Figure 8 (B).

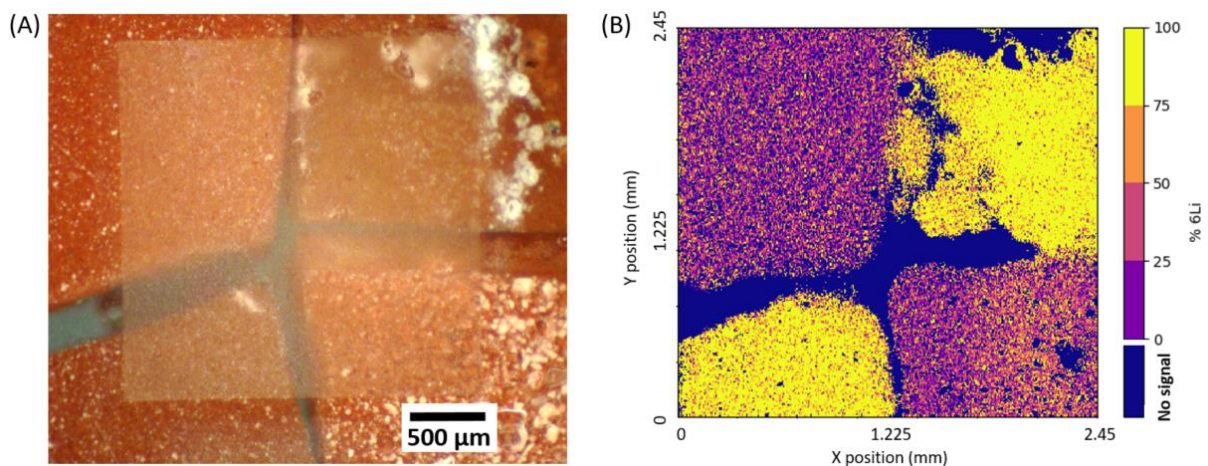


Figure 8: (A) picture of the sample surface after the analysis taken using a binocular magnifier, the visible square corresponds to the ablated matrix, (B) LIBS mapping of the  ${}^6\text{Li}$  isotopic abundance with a 575 counts intensity threshold, 350\*350 laser shots with a 7  $\mu\text{m}$  step

On the LIBS lithium isotopic mapping, lithium is not always detected, even in lithium-containing epoxy parts. This may be due to remaining air bubbles during the sample preparation steps, or to a lower lithium concentration inducing a signal lower than the threshold.

The lithium-containing parts are also not fully homogeneous, which is not quite surprising as the relative uncertainty in concentration is higher than the color bars steps (every 25%).

The orange spots in the 95.5%  ${}^6\text{Li}$  epoxy parts (yellow parts of the mapping) are more present in the border of the mapping, where the laser shot ablates less lithium. It means that a red shift of the emission line occurs, in accordance with an assumed decrease of the plasma density.

Figure 8 shows that it is feasible to perform fast and semi-quantitative lithium isotopic mapping using LIBS technique with a 3.3  $\mu\text{m}$  lateral resolution on epoxy samples containing lithium carbonate. A 40% relative uncertainty on the  ${}^6\text{Li}$  isotopic abundance for single-shots measurements at 95% confidence was obtained. Compared to other analytical techniques, LIBS for lithium isotopic analysis is

less precise than ToF-SIMS [1,17], LA-MC-ICP-MS [16] and NanoSIMS [19] on the  $^6\text{Li}$  isotopic abundance with a worse surface resolution, however it allows faster analysis on bigger surfaces. The obtained uncertainty on the  $^6\text{Li}$  isotopic abundance is relatively high, but it is enough to study large isotopic variations, e.g. for isotopic labeling experiments in solids. Several ways of improvement to decrease this uncertainty could be implemented, such as a shot-to-shot pulse energy correction [36] or by increasing the plasma emission collection efficiency to improve the signal-to-noise ratio.

#### 4. Conclusion

LIBS enables to perform lithium isotopic analysis in solid samples. In this paper, we developed this technique for depth profile measurements with a 9% relative uncertainty on the  $^6\text{Li}$  isotopic abundance with 0.74  $\mu\text{m}$  depth resolution. The first high-resolution surface lithium isotopic mapping obtained by LIBS with a 3.3  $\mu\text{m}$  lateral resolution and 40% relative uncertainty on the  $^6\text{Li}$  isotopic abundance was presented.

This work opens ways to a lot of possibilities for spatially-resolved studies of lithium isotopic abundance in solid samples by using LIBS. As an example, a proof-of-concept of LIBS application to the study of lithium isotopic labelling in solid-state electrolytes of lithium batteries was already described [36]. This paper, by presenting the incorporation of the spatial information to LIBS for lithium isotopic analysis, opens the way to lithium isotopic tracing in solid-state batteries using depth profile measurements and high-resolution mappings. Therefore, our future work will address this issue, particularly in order to analyze the interfaces in solid-state batteries and to study the lithium transport during or after electrochemical cycling.

#### 5. Declaration of competing interest

None

#### 6. Acknowledgement

We thank Nicolas Lochet for his assistance on the preparation of lithium carbonate pellets. We also thank Thomas Meyer and Thibaut Gutel for their precious advice.

#### 7. References

- [1] T. Meyer, T. Gutel, H. Manzanarez, M. Bardet, E. De Vito, Lithium Self-Diffusion in a Polymer Electrolyte for Solid-State Batteries: ToF-SIMS/ssNMR Correlative Characterization and Modeling Based on Lithium Isotopic Labeling, *ACS Appl. Mater. Interfaces*. 15 (2023) 44268–44279. <https://doi.org/10.1021/acsami.3c08829>.
- [2] S. Lou, Z. Yu, Q. Liu, H. Wang, M. Chen, J. Wang, Multi-scale Imaging of Solid-State Battery

- Interfaces: From Atomic Scale to Macroscopic Scale, *Chem.* 6 (2020) 2199–2218.  
<https://doi.org/10.1016/j.chempr.2020.06.030>.
- [3] M. Diehl, M. Evertz, M. Winter, S. Nowak, Deciphering the lithium ion movement in lithium ion batteries: determination of the isotopic abundances of  $^6\text{Li}$  and  $^7\text{Li}$ , *RSC Adv.* 9 (2019) 12055–12062. <https://doi.org/10.1039/C9RA02312G>.
- [4] R.C. MacHado, D.F. Andrade, D. V. Babos, J.P. Castro, V.C. Costa, M.A. Sperança, J.A. Garcia, R.R. Gamela, E.R. Pereira-Filho, Solid sampling: Advantages and challenges for chemical element determination- A critical review, *J. Anal. At. Spectrom.* 35 (2020) 54–77.  
<https://doi.org/10.1039/c9ja00306a>.
- [5] L. Wang, X. Xing, X. Zeng, S.R.E. Jackson, T. TeSlaa, O. Al-Dalahmah, L.Z. Samarah, K. Goodwin, L. Yang, M.R. McReynolds, X. Li, J.J. Wolff, J.D. Rabinowitz, S.M. Davidson, Spatially resolved isotope tracing reveals tissue metabolic activity, *Nat. Methods.* 19 (2022) 223–230.  
<https://doi.org/10.1038/s41592-021-01378-y>.
- [6] E. Bolea-Fernandez, S.J.M. Van Malderen, L. Balcaen, M. Resano, F. Vanhaecke, Laser ablation-tandem ICP-mass spectrometry (LA-ICP-MS/MS) for direct Sr isotopic analysis of solid samples with high Rb/Sr ratios, *J. Anal. At. Spectrom.* 31 (2016) 464–472.  
<https://doi.org/10.1039/c5ja00404g>.
- [7] U. Schaltegger, A.K. Schmitt, M.S.A. Horstwood, U-Th-Pb zircon geochronology by ID-TIMS, SIMS, and laser ablation ICP-MS: Recipes, interpretations, and opportunities, *Chem. Geol.* 402 (2015) 89–110. <https://doi.org/10.1016/j.chemgeo.2015.02.028>.
- [8] D. Chew, K. Drost, J.H. Marsh, J.A. Petrus, LA-ICP-MS imaging in the geosciences and its applications to geochronology, *Chem. Geol.* 559 (2021) 119917.  
<https://doi.org/10.1016/j.chemgeo.2020.119917>.
- [9] M. Krachler, M. Wallenius, A. Nicholl, K. Mayer, Spatially-resolved uranium isotopic analysis of contaminated scrap metal using laser ablation multi-collector ICP-MS, *RSC Adv.* 10 (2020) 16629–16636. <https://doi.org/10.1039/d0ra02899a>.
- [10] J. Pisonero, Glow discharge spectroscopy for depth profile analysis: From micrometer to sub-nanometer layers, *Anal. Bioanal. Chem.* 384 (2006) 47–49. <https://doi.org/10.1007/s00216-005-0143-1>.
- [11] F. Chartier, M. Tabarant, Spectrométrie de masse à décharge luminescente GDMS, *Tech. l'ingénieur.* 33 (2008) 10–13.

- [12] L.A. Rush, J.B. Cliff, D.D. Reilly, A.M. Duffin, C.S. Menoni, Extreme ultraviolet laser ablation mass spectrometry for chemical mapping at the nanoscale, 2021 IEEE Photonics Conf. IPC 2021 - Proc. (2021) 1–2. <https://doi.org/10.1109/IPC48725.2021.9592924>.
- [13] L.A. Rush, J.B. Cliff, D.D. Reilly, A.M. Duffin, C.S. Menoni, Imaging isotopic content at the nanoscale using extreme ultraviolet laser ablation and ionization mass spectrometry, in: D. Bleiner (Ed.), Int. Conf. X-Ray Lasers 2020, SPIE, 2021: p. 15. <https://doi.org/10.1117/12.2593315>.
- [14] A. Devaraj, B. Matthews, B. Arey, L. Bagaasen, E. Buck, G. Sevigny, D. Senor, Neutron irradiation induced changes in isotopic abundance of  $^6\text{Li}$  and  $^3\text{D}$  nanoscale distribution of tritium in  $\text{LiAlO}_2$  pellets analyzed by atom probe tomography, Mater. Charact. 176 (2021) 111095. <https://doi.org/10.1016/j.matchar.2021.111095>.
- [15] S.M. Reddy, D.W. Saxey, W.D.A. Rickard, D. Fougereuse, S.D. Montalvo, R. Verberne, A. van Riessen, Atom Probe Tomography: Development and Application to the Geosciences, Geostand. Geoanalytical Res. 44 (2020) 5–50. <https://doi.org/10.1111/ggr.12313>.
- [16] L.K. Steinmann, M. Oeser, I. Horn, H.-M. Seitz, S. Weyer, In situ high-precision lithium isotope analyses at low concentration levels with femtosecond-LA-MC-ICP-MS, J. Anal. At. Spectrom. 34 (2019) 1447–1458. <https://doi.org/10.1039/C9JA00088G>.
- [17] M. Berthault, Etude de la dynamique du lithium dans un système électrochimique Li-ion par traçage isotopique en combinant les spectrométries RMN et ToF-SIMS, 2021.
- [18] W. Yang, S. Hu, J.C. Zhang, J.L. Hao, Y.T. Lin, NanoSIMS analytical technique and its applications in earth sciences, Sci. China Earth Sci. 58 (2015) 1758–1767. <https://doi.org/10.1007/s11430-015-5106-6>.
- [19] F. Jia, X. Zhao, Y. Zhao, Advancements in ToF-SIMS imaging for life sciences, Front. Chem. 11 (2023) 1–15. <https://doi.org/10.3389/fchem.2023.1237408>.
- [20] T. Wang, X. Cheng, H. Xu, Y. Meng, Z. Yin, X. Li, W. Hang, Perspective on Advances in Laser-Based High-Resolution Mass Spectrometry Imaging, Anal. Chem. 92 (2020) 543–553. <https://doi.org/10.1021/acs.analchem.9b04067>.
- [21] K. Li, J. Liu, C.R.M. Grovenor, K.L. Moore, NanoSIMS Imaging and Analysis in Materials Science, Annu. Rev. Anal. Chem. 13 (2020) 273–292. <https://doi.org/10.1146/annurev-anchem-092019-032524>.
- [22] A. Donard, F. Pointurier, A.-C. Pottin, A. Hubert, C. Pécheyran, Determination of the isotopic

- composition of micrometric uranium particles by UV femtosecond laser ablation coupled with sector-field single-collector ICP-MS, *J. Anal. At. Spectrom.* 32 (2017) 96–106.  
<https://doi.org/10.1039/C6JA00071A>.
- [23] P. Harte, M. Evertz, T. Schwieters, M. Diehl, M. Winter, S. Nowak, Adaptation and improvement of an elemental mapping method for lithium ion battery electrodes and separators by means of laser ablation-inductively coupled plasma-mass spectrometry, *Anal. Bioanal. Chem.* 411 (2019) 581–589. <https://doi.org/10.1007/s00216-018-1351-9>.
- [24] A. Priebe, A. Aribia, J. Sastre, Y.E. Romanyuk, J. Michler, 3D High-Resolution Chemical Characterization of Sputtered Li-Rich NMC811 Thin Films Using TOF-SIMS, *Anal. Chem.* 95 (2023) 1074–1084. <https://doi.org/10.1021/acs.analchem.2c03780>.
- [25] E. Darque-Ceretti, M. Aucouturier, P. Lehuédé, Spectrométrie de masse d'ions secondaires : SIMS et ToF-SIMS- Principes et appareillages, *Tech. l'ingénieur.* 33 (2014).
- [26] R.N.S. Sodhi, Time-of-flight secondary ion mass spectrometry (TOF-SIMS):—versatility in chemical and imaging surface analysis, *Analyst.* 129 (2004) 483–487.  
<https://doi.org/10.1039/B402607C>.
- [27] B.W. Smith, I.B. Gornushkin, L.A. King, J.D. Winefordner, Laser ablation-atomic fluorescence technique for isotopically selective determination of lithium in solids, *Spectrochim. Acta, Part B At. Spectrosc.* 53 B (1998) 1131–1138. [https://doi.org/10.1016/s0584-8547\(98\)00132-3](https://doi.org/10.1016/s0584-8547(98)00132-3).
- [28] J. Merten, B. Johnson, Laser continuum source atomic absorption spectroscopy: Measuring the ground state with nanosecond resolution in laser-induced plasmas, *Spectrochim. Acta - Part B At. Spectrosc.* 139 (2018) 38–43. <https://doi.org/10.1016/j.sab.2017.11.006>.
- [29] G. Hull, E.D. McNaghten, P. Coffey, P. Martin, Isotopic analysis and plasma diagnostics for lithium detection using combined laser ablation–tunable diode laser absorption spectroscopy and laser-induced breakdown spectroscopy, *Spectrochim. Acta Part B At. Spectrosc.* 177 (2021) 106051. <https://doi.org/10.1016/j.sab.2020.106051>.
- [30] E.J. Kautz, A. Xu, A. V. Harilal, M.P. Polek, A.M. Casella, D.J. Senor, S.S. Harilal, Influence of ambient gas on self-reversal in Li transitions relevant to isotopic analysis, *Opt. Express.* 31 (2023) 3549. <https://doi.org/10.1364/OE.477990>.
- [31] J.C. Wood, M.B. Shattan, Lithium Isotope Measurement Using Laser-Induced Breakdown Spectroscopy and Chemometrics, *Appl. Spectrosc.* 75 (2021) 199–207.  
<https://doi.org/10.1177/0003702820953205>.

- [32] D.A. Cremers, A. Beddingfield, R. Smithwick, R.C. Chinni, C. Randy Jones, B. Beardsley, L. Karch, Monitoring uranium, hydrogen, and lithium and their isotopes using a compact laser-induced breakdown spectroscopy (LIBS) probe and high-resolution spectrometer, *Appl. Spectrosc.* 66 (2012) 250–261. <https://doi.org/10.1366/11-06314>.
- [33] S.S. Harilal, B.E. Brumfield, N.L. LaHaye, K.C. Hartig, M.C. Phillips, Optical spectroscopy of laser-produced plasmas for standoff isotopic analysis, *Appl. Phys. Rev.* 5 (2018) 021301. <https://doi.org/10.1063/1.5016053>.
- [34] K. Touchet, F. Chartier, J. Hermann, J.-B. Sirven, Laser-induced breakdown self-reversal isotopic spectrometry for isotopic analysis of lithium, *Spectrochim. Acta - Part B At. Spectrosc.* 168 (2020) 105868. <https://doi.org/10.1016/j.sab.2020.105868>.
- [35] K. Touchet, *Analyse isotopique directe des solides par spectroscopie des plasmas d'ablation laser*, 2020.
- [36] D. Gallot-Duval, T. Meyer, C. Quéré, T. Gutel, E. De Vito, J.-B. Sirven, High-resolution isotopic analysis of lithium by micro laser-induced breakdown self-reversal isotopic spectrometry (LIBRIS) for isotopic labelling of lithium in solid-state electrolyte of lithium batteries, *Spectrochim. Acta Part B At. Spectrosc.* 206 (2023) 106731. <https://doi.org/10.1016/j.sab.2023.106731>.
- [37] J. Walls, R. Ashby, J.J. Clarke, B. Lu, W.A. van Wijngaarden, Measurement of isotope shifts, fine and hyperfine structure splittings of the lithium D lines, *Eur. Phys. J. D.* 22 (2003) 159–162. <https://doi.org/10.1140/epjd/e2003-00001-5>.
- [38] R.H. Hughes, Isotope Shift in the First Spectrum of Atomic Lithium, *Phys. Rev.* 99 (1955) 1837–1839. <https://doi.org/10.1103/PhysRev.99.1837>.
- [39] C.J. Sansonetti, B. Richou, R. Engleman, L.J. Radziemski, Measurements of the resonance lines of <sup>6</sup>Li and <sup>7</sup>Li by Doppler-free frequency-modulation spectroscopy, *Phys. Rev. A.* 52 (1995) 2682–2688. <https://doi.org/10.1103/PhysRevA.52.2682>.
- [40] D.W. Hahn, N. Omenetto, Laser-induced breakdown spectroscopy (LIBS), part I: Review of basic diagnostics and plasmaparticle interactions: Still-challenging issues within the analytical plasma community, *Appl. Spectrosc.* 64 (2010) 335–366. <https://doi.org/10.1366/000370210793561691>.
- [41] M.P. Mateo, G. Nicolas, V. Piñon, A. Yañez, Improvements in depth-profiling of thick samples by laser-induced breakdown spectroscopy using linear correlation, *Surf. Interface Anal.* 38

(2006) 941–948. <https://doi.org/10.1002/sia.2352>.

- [42] B.T. Manard, H.B. Andrews, C.D. Quarles, V.C. Bradley, P. Doyle, N.A. Zirakparvar, D.R. Dunlap, C.R. Hexel, Exploration of LIBS as a novel and rapid elemental mapping technique of nuclear fuels in the form of surrogate TRISO particles, *J. Anal. At. Spectrom.* 38 (2023) 1412–1420. <https://doi.org/10.1039/d3ja00034f>.